Journal of Electroanalytical Chemistry 780 (2016) 373–378

Contents lists available at ScienceDirect

Journal of Electroanalytical Chemistry

journal homepage: www.elsevier.com/locate/jelechem

Photoelectrochemical activity of colloidal TiO_2 nanostructures assembled at polarisable liquid/liquid interfaces

Daniela Plana *, David J. Fermín

School of Chemistry, University of Bristol, Cantocks Close, Bristol BS8 1TS, UK

ARTICLE INFO

Article history:
Received 1 July 2015
Received in revised form 21 September 2015
Accepted 22 September 2015
Available online 25 September 2015

Keywords:
Photocurrent
Liquid/liquid interfaces
TiO_2 nanoparticles
Ferrocene

ABSTRACT

Photoelectrochemical responses arising from the heterogeneous hole-transfer from colloidal TiO_2 nanoparticles to ferrocene species across the polarizable water/1,2-dichloroethane (DCE) interface are investigated as a function of the formal redox potential of the electron donor. The interfacial assembly of electrostatically stabilized 5 nm TiO_2 colloids was monitored by impedance measurements at various Galvani potential difference across the liquid/liquid interface. The onset potential of the photocurrent responses is close to the potential at which the excess interfacial charge increases due to the assembly of the TiO_2 nanoparticles. However, a closer examination of the potential dependence of these two parameters show that the interfacial excess charge is not solely dependent on the adsorption of charged nanoparticles at the interface. We also provide strong evidence that the photoelectrochemical responses are determined by the relationship between rate of electron capture at the nanoparticle surface and surface recombination processes, rather than the interfacial oxidation of the ferrocene derivatives. Second order surface recombination constants of the order of 10^{-3} cm^2 s^{-1} were estimated, which are consistent with a ~0.6 quantum yield for the heterogenous hole-transfer.

1. Introduction

Polarisable interfaces between two immiscible liquids (ITIES) are a highly versatile platform for investigating a wide range of interfacial processes promoted by illumination, including heterogeneous quenching, homogeneous photoreaction coupled to ion transfer and charge transfer at solid electrodes coupled to ion transfer across polarizable liquid/liquid boundaries [1–8]. Recent investigations have looked at a variety of complex multi-electron transfer reactions at the ITIES employing fully molecular redox active species [9–11]. In this sense, it could be argued that introducing colloidal nanomaterials (*e.g.* metal or semiconductor nanoparticles) can introduce more profound effects in interfacial reactivity as a result of significant changes in the electronic density of states. Indeed, potential-induced assembly of nanostructures at the polarizable ITIES is a highly elegant approach to tuning the reactivity of this molecular interfaces which has been largely unexplored.

Photocurrent responses originating from heterogeneous quenching of dyes assembled at the ITIES have provided fundamental insights on the potential dependence of heterogeneous electron transfer across these systems [12–14]. Eugster et al. have shown that the potential dependence of the effective heterogeneous electron transfer rate constant involving self-assembled water soluble porphyrins and a range of ferrocene derivatives can be described on the basis of the Marcus formalism [15]. In the case of molecular species, the dynamics of heterogeneous electron transfer is mainly determined by the distance separating redox donor and acceptors, which translate into solvent reorganization energies of the order of 1 eV [13,15,16]. Based on the Marcus model for electron transfer [17–19], these reorganization energy values are consistent with an effective distance separating the redox species of approximately 1 nm, assuming a molecularly sharp liquid/liquid boundary layer. This point raises the question of whether these considerations apply to nanoparticles exhibiting dimensions similar or larger than this electron transfer length scale.

In the present paper, we investigate dynamic aspects associated with interfacial hole transfer of TiO_2 nanostructures to ferrocene derivatives across the polarizable water/DCE interface. As demonstrated previously, colloidal TiO_2 nanoparticles can be assembled at the liquid/liquid interface depending on the pH of the aqueous solution and the Galvani potential difference [20,21]. Our results show that the magnitude and potential dependence of the incident-photon-to-current (IPCE) is essentially unaffected by the formal redox potential of the ferrocene derivatives. We conclude that the rate limiting step of the interfacial photochemical event is linked to the lifetime of the radical intermediates, determined by the relationship between electron capture by species in the aqueous phase (oxygen) and surface recombination processes, rather than the heterogeneous charge transfer across the liquid/liquid boundary.

Abbreviations: AcFc, Acetylferrocene; BTPPA-TPFB, bis(triphenylphosphoranylidene) ammonium tetrakis(pentafluorophenyl)borate; DCE, 1,2-dichloroethane; DMFc, 1,1′-dimethylferrocene; E_{pzc}, potential at point of zero charge; Fc, ferrocene; %IPCE, incident photon to current conversion efficiency; ITIES, interfaces between two immiscible liquids; I_0, incident photon-flux; j_{photo}, photocurrent.

* Corresponding author.
E-mail addresses: d.plana@bristol.ac.uk (D. Plana), david.fermin@bristol.ac.uk (D.J. Fermín).

http://dx.doi.org/10.1016/j.jelechem.2015.09.030

2. Methods

A custom made three-compartment electrochemical cell was used in all experiments, featuring two separate compartments for the organic and aqueous reference electrodes connected to the main compartment *via* with Luggin capillaries. The main compartment sustained the water/DCE interface with a geometric area of 2.27 cm^2. Illumination was performed through the bottom of the cell, *i.e.* through the organic electrolyte, *via* a quartz window. The cell composition used throughout is shown in Scheme 1, where the organic electrolyte is bis(triphenylphosphoranylidene)ammonium tetrakis(pentafluorophenyl)borate (BTPPA-TPFB), which was synthesized *via* a simple metathesis reaction of bis(triphenylphosphoranylidene)ammonium chloride and potassium tetrakis(pentafluorophenyl)borate (1:1 M ratio) in a 2:1:1 mixture of acetone:ethanol:water, with re-crystallization performed in acetone [22].

Full details on the synthesis and characterization of the TiO_2 nanoparticles can be found in the Supporting Information, SI. Briefly, $TiCl_4$ was hydrolysed in an ice-cold bath, resulting in a fairly monodisperse, electrostatically stabilized colloidal suspension of spherical 5.2 ± 1.1 nm diameter TiO_2 nanoparticles, with an average particle charge of 3.3×10^{-19} C at pH 3, in agreement with previous studies [20,23].

Electrochemical and photoelectrochemical studies were performed with a PGSTAT302N (Autolab) and a Compactstat (Ivium), respectively, both fitted with frequency response analysers. A lock-in amplifier and a function generator (Stanford Research Systems), controlled *via* a LabView interface programme written in-house were used in the measurement of photoresponses. Light perturbation was introduced with a light emitting diode (Thorlabs) with an emission centred at 311 nm (with a linear power output between 6.06 μW and 0.93 mW, which equates to photon-fluxes between 0.1 and 14.6×10^{14} s^{-1}). The absorption coefficient of the titania nanoparticles at this wavelength was estimated to be 7.0 ± 0.3 g^{-1} L cm^{-1}.

3. Results and discussion

Fig. 1a shows cyclic voltammograms performed with the cell described in Scheme 1 in the absence of ferrocene derivatives in the organic phase. It can be seen that, particularly on the positive side of the potential scale, the capacitive currents increase when the titania nanoparticles are introduced in the aqueous phase. The ideally polarizable potential range, determined by the transfer of aqueous electrolyte species, remains unaffected with increasing titania concentration. The applied potential is referred against the apparent potential of zero charge (E_{pzc}) of the liquid/liquid interface. E_{pzc} is defined as the potential of minimum interfacial capacitance in the presence of only background electrolytes. In terms of the Galvani potential difference based on the tetramethylammonium formal transfer potential, the E_{pzc} for this system has been reported to be shifted approximately 0.03 V [20]. Although some deviations can be found between the minimum capacitance and the true value of E_{pzc}, due to non-ideal polarization and Faradaic processes, they are minimized at low electrolyte concentrations and in the absence of species that adsorb at or transfer across the interface [24].

Fig. 1b shows the differential capacitance as a function of applied potential with increasing titania concentration in the aqueous phase. These values are taken from impedance measurements at a frequency of 1 Hz, with a 10 mV amplitude, assuming a simple *RC* circuit within the ideally polarizable window. The observed increase in interfacial

Ag	AgCl	(x mg L^{-1} TiO_2) 0.01 M LiCl (aq) pH 2.5	‖	(1.0 mM Fc/DMFc/AcFc) 5.0 mM BTPPA-TPFB (DCE)	1.0 mM BTPPACl 0.01 M LiCl (aq)	AgCl	Ag

Scheme 1. Cell composition used in liquid/liquid electrochemical and photoelectrochemical studies. The TiO_2 in the aqueous phase and the ferrocenes in the DCE are in brackets, as they are present or absent in different experiments.

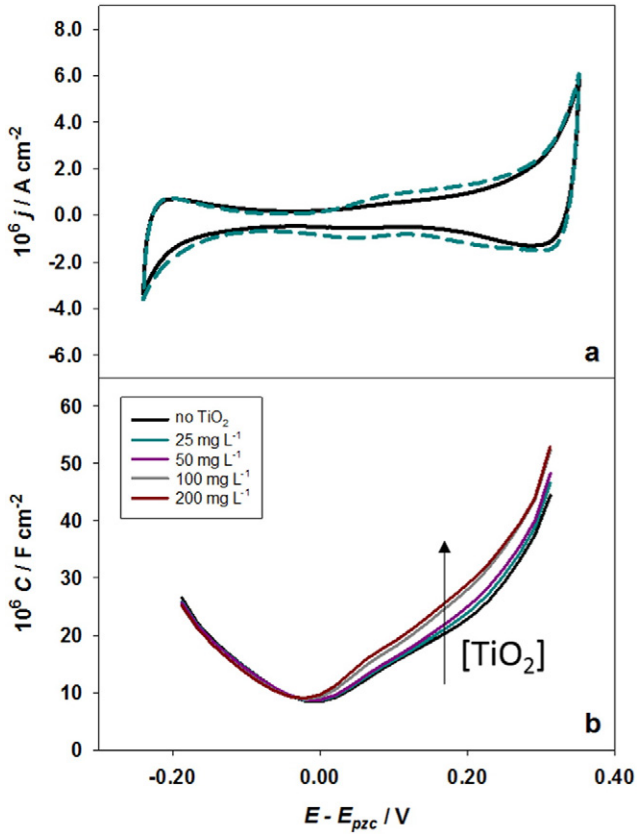

Fig. 1. Cyclic voltammetry (a) performed in the cell described in Scheme 1, in the presence (dashed cyan) and absence (solid black) of TiO_2 nanoparticles in the aqueous phase. Capacitance as a function of applied potential (b), with increasing capacitance observed as the concentration of TiO_2 increases from zero (black) to 200 mg L^{-1} in the bulk aqueous phase (wine). The arrow indicates increasing titania concentration.

capacitance as the potential is increased in the presence of titania nanoparticles can be rationalized in terms of the potential induced assembly of the positively charged colloids upon interfacial polarization [20]. The potential dependence of the capacitance is fully reversible upon consecutive cycles, demonstrating that the nanoparticle surface excess can be tuned by the electrical polarization.

The excess charge (Q) at the liquid/liquid interface as a function of the applied potential estimated by integration of the differential capacitance is shown in Fig. 2a. The boundary conditions used in this analysis involved that (i) the excess charge is zero at E_{pzc} in the absence of titania nanoparticles and (ii) the excess charge at the negative end of the potential window is independent of the titania concentration. Both approximations have been proven valid in previous studies associated with potential induced assembly of nanoparticles [20–22]. It can be seen that as the titania concentration increases, the excess charge increases across the whole potential range. This trend can be seen more clearly in Fig. 2b, which displays the excess charge after subtraction of the interfacial charge in the absence of titania nanoparticles. This approach implicitly decouples the potential induced assembly of the colloidal nanoparticles from the concentration polarization of the supporting electrolyte. The excess charge can be expressed as surface excess of titania nanoparticles (Fig. 2c) by assuming that the surface charge obtained from mobility measurements is unaffected by the interfacial polarization or local pH changes. Although the nanoparticle surface excess shows a monotonic increase with increasing applied potential, the trend shows a saturation with increasing titania concentration at a given potential. This puzzling behaviour suggest that the correlation between excess interfacial charge (Q_{diff}) and surface particle

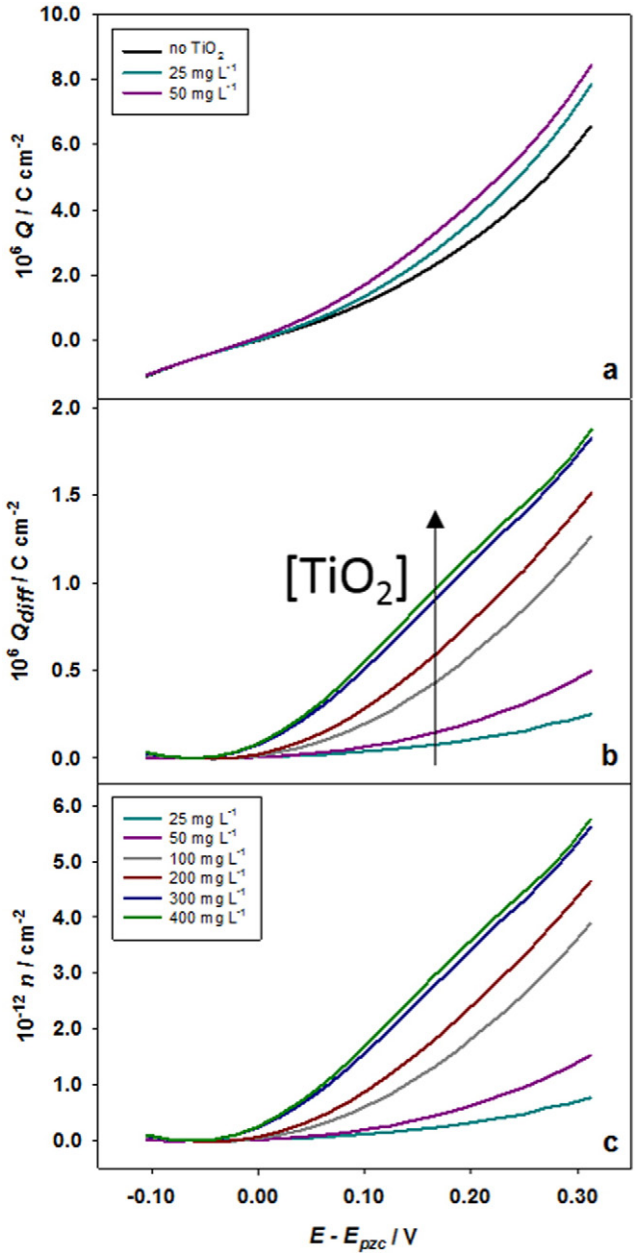

Fig. 2. Excess charge (Q) at the interface as a function of potential obtained from integrating the interfacial capacitance in the absence and presence of TiO_2 (a). Excess charge for various TiO_2 colloid concentrations (Q_{diff}) after subtraction of excess charge of the background electrolyte (b). The excess charge associated with TiO_2 particles exhibits an onset potential close to E_{pzc}, becoming weakly concentration dependent for values above 300 mg L^{-1}.The arrow indicates increasing titania concentration. Apparent TiO_2 particle number density (n) estimated assuming a potential independent particle charge of $+3.3 \times 10^{-19}$ C (c).

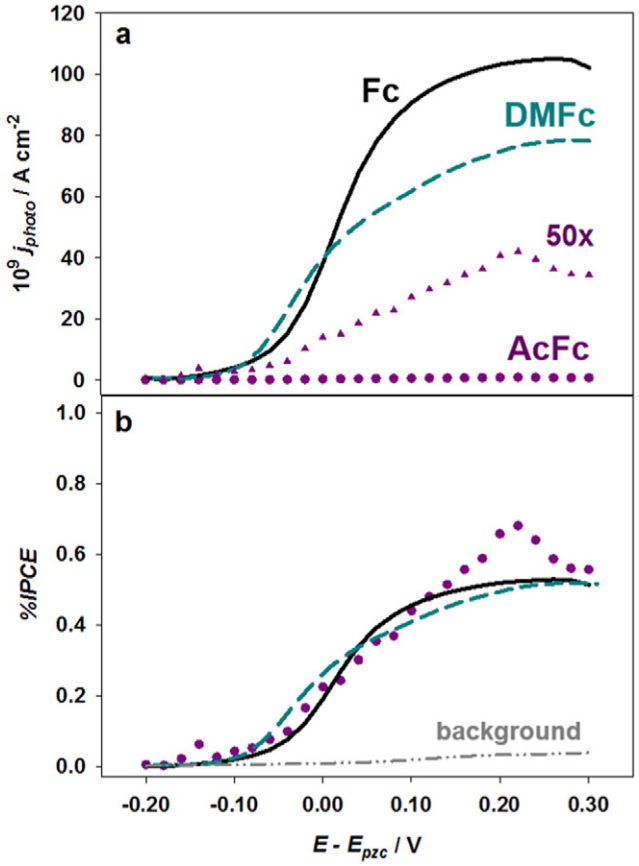

Fig. 3. Magnitude of photocurrent density (j_{photo}, peak-to-peak) under square wave perturbation (0.05 Hz and 4.7×10^{14} cm^{-2} s^{-1}, uncorrected for absorption) and lock-in detection in the presence of Fc, DMFc and AcFc (a); the purple triangles denote the photocurrent in the presence of AcFc oxidation multiplied by a factor of 50. Incident-photon-to-current-efficiency (IPCE) as a function of the applied potential after correction by absorption of the organic electrolyte (b). The background photoresponse obtained in the absence of any ferrocene species is shown in the grey dash-dotted trace.

concentration (n) is non-linear. We will elaborate on this point further below in the discussion.

Fig. 3a shows photocurrent-potential curves obtained in the presence of ferrocene (Fc), 1,1′-dimethylferrocene (DMFc) and acetylferrocene (AcFc). Experiments were carried out employing lock-in detection under a square wave light perturbation of 4.7×10^{14} cm^{-2} s^{-1} (uncorrected for absorption in the electrochemical cell) and a frequency of 0.05 Hz. The curves in Fig. 4a represent the amplitude of the photocurrent response, while the phase value remains very small except for at potentials close to the end of the polarizable window. While the photocurrent magnitude was larger in the presence of Fc, the potential dependence was very similar for all three electron donors. Fig. 3b shows the potential dependence of the incident-photon-to-current efficiency (IPCE) considering the attenuation of the photon-flux introduced by the ferrocene derivative. It can be seen that even if the photocurrent magnitude is orders of magnitude smaller in the case of AcFc with respect to Fc, the IPCE values are comparable. This is essentially due to the fact that AcFc exhibits a strong absorbance at 311 nm. The corresponding absorption spectra of the various electron donors are included in the Supporting Information. Furthermore, IPCE values below 1% are consistent with the light capture cross-section of a quasi 2D assembly of TiO_2 colloids at the liquid/liquid interface. Fig. 3b also shows the small photoresponses arising from reactions in the absence of Fc derivatives. Preliminary studies suggest that these responses are associated with the oxidation of the organic electrolyte.

A remarkable aspect of these trends is the fact that IPCE values and photocurrent onset potentials (close to −0.10 V *vs* E_{pzc}) are very similar for all three donor species, despite the significant difference in terms of formal redox potentials. As shown in the supporting information, the formal redox potentials of DMFc and AcFc are −0.13 and 0.28 V *vs* the potential of Fc. This behaviour is in stark contrast to trends observed for water-soluble porphyrins and CdSe quantum dots assemblies at the water/DCE interface, where the potential dependence and magnitude of the photocurrent are strongly dependent of the donor redox potential [13,25]. Consequently, we can postulate that the photocurrent kinetics are not limited by the rate of heterogeneous electron transfer across the liquid/liquid interface.

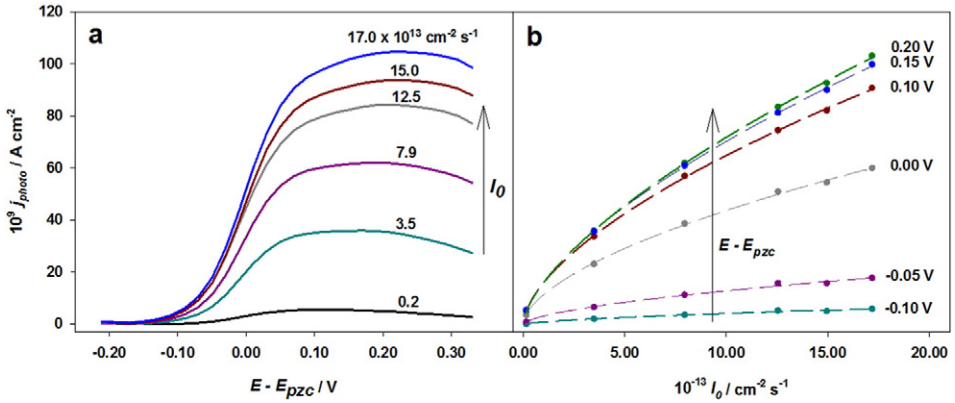

Fig. 4. Photocurrent-potential curves in the presence of Fc at various incident photon-fluxes (a). The arrow indicates increasing incident photon-flux (I_0, considering attenuation by the organic phase). The TiO_2 colloid concentration was 400 mg L^{-1}. Photocurrent as a function of incident photon-flux at various applied potentials (b). A square-root dependence is found at potentials more positive than −0.10 V, as shown by the dashed lines. The arrow indicates increasingly positive applied potentials ($E - E_{pzc}$).

The dependence of the photocurrent on the incident photon-flux (corrected for absorption of the organic phase) in the presence of Fc is exemplified in Fig. 4a. Although the magnitude of the photocurrent increases with increasing incident photon-flux, the photocurrent onset potential and overall potential dependence remain essentially unaffected. Furthermore, the light intensity dependence of the photocurrent is non-linear as illustrated in Fig. 4b. This deviation from linearity indicates that the quantum yield associated with the heterogeneous photoreaction is not 1, due to the presence of recombination phenomena. The quantum yield (Φ) is defined by the ratio of absorbed light that is transformed into photocurrent, as expressed by Eq. (1), where σ corresponds to the optical capture cross section at 311 nm (from UV–visible spectroscopic analysis $\sigma = 2.2 \times 10^{-15}$ cm^2).

$$\Phi = \frac{j_{photo}}{qn\sigma I_0}. \tag{1}$$

The mechanism associated with the photocurrent responses can be expressed in terms of a series of elementary steps involving hole trapping by OH radicals at the TiO_2 surface (Eq. (3)), heterogeneous electron transfer involving the ferrocene derivatives (Eq. (4)), electron capture by species in the aqueous electrolyte (Eq. (6), in this case likely oxygen reduction) and carrier recombination *via* OH radical at the surface of the assembled TiO_2 colloid (Eq. (5)) [20].

$$TiO2 \xrightarrow{h\nu} e^-_{CB} + h^+_{VB}. \tag{2}$$

$$h^+ + OH^- \xrightarrow{k_1} OH^{\cdot}. \tag{3}$$

$$OH^{\cdot} + Fc \xrightarrow{k^{II}_{et}} Fc^+ + OH^-. \tag{4}$$

$$e^- + OH^{\cdot} \xrightarrow{k_2} OH^-. \tag{5}$$

$$e^- + X \xrightarrow{k^{II}_3} X^-. \tag{6}$$

Under steady-state condition, the photocurrent responses can be expressed as:

$$j_{photo} = qk^{II}_{et}[Fc][OH^{\cdot}] = qk_{et}[OH^{\cdot}] \tag{7}$$

where $k_{et} = k^{II}_{et}[Fc]$. From Eqs. (1) to (5), the steady state concentration of $OH^{\cdot}$ at the interface is given by the following quadratic relation:

$$\frac{k_2 k_{et}}{k_3}[OH^{\cdot}]^2 + k_{et}[OH^{\cdot}] - I_0\sigma n = 0 \tag{8}$$

where $k_3 = k^{II}_3[X]$. The concentration terms relates to the steady values across the interfacial region. In the limiting case where electron capture (most probably by oxygen) is significantly faster than recombination, *i.e.* $k_2[OH^{\cdot}] \ll k_3$, the photocurrent will exhibit a linear dependence on the incident photon-flux (Eq. (9)). This limiting case corresponds to a quantum yield of $\Phi = 1$. However, the trend shown in Fig. 4b demonstrates that recombination is not negligible under the experimental conditions. A second limiting case can be defined in terms of $k_2[OH^{\cdot}_s] \gg k_3$, resulting in a square root dependence of the j_{photo} with I_0 as described by Eq. (10). This relationship appears more consistent with the experimental trends in Fig. 4.

$$j_{photo} = qI_0\sigma n. \tag{9}$$

$$\frac{j_{photo}}{q} = \sqrt{\frac{k_3 k_{et} I_0 \sigma n}{k_2}}. \tag{10}$$

Fig. 5 estimates the particle number density and interfacial coverage as a function of the applied potential from the photocurrent responses employing Eqs. (7) and (8). It is clear that a quantitative analysis of these parameters solely based on photocurrent potential curves is not possible given the number of rate constants associated with the various elementary steps involved. In this case, we have considered rate constants of $k_{et} \sim 10^4$ s^{-1}, based on studies involving self-assembled porphyrins at the water/DCE interface [13,26], and $k_3 \sim 7 \times 10^4$ s^{-1}, taken from the work by Bahnemann et al. who measured the rate constant for oxygen capture by TiO_2 (mediated by deep trap states) [27]. The curves presented were estimated for values of k_2 ranging from 1×10^{-5} to 1×10^{-2} cm^2 s^{-1}.

The first value (1×10^{-5} cm^2 s^{-1}) coincides with the behaviour obtained from the limiting case expressed in Eq. (9), where recombination has very little effect and thus $\Phi = 1$; however, this extreme has already been disproven by the non-linear dependence of j_{photo} *vs* I_0 (Fig. 4b). As the value of k_2 is increased, higher particle number densities are obtained, with a concomitant decrease in quantum yield. Interfacial coverages much higher than 1 constitute an unlikely scenario given that it will require carrier transport across several layers of titania nanoparticles. This could only happen if there is close interaction between particles at the interface, which will inevitably lead to de-stabilization of the colloidal suspension. The trends simulated in Fig. 5 suggests that the second order surface recombination rate k_2 in this system is of the order of ~10^{-3} cm^2 s^{-1}. This value can be contrasted with second order recombination rate constants for TiO_2 nanoparticles of similar size as probed by time-resolved pump-probe spectroscopy, typically in the range of 1×10^{-11} to 2×10^{-10} cm^3 s^{-1} [28–30]. Considering the small dimension of these particles, it is expected that charge carriers will diffuse to

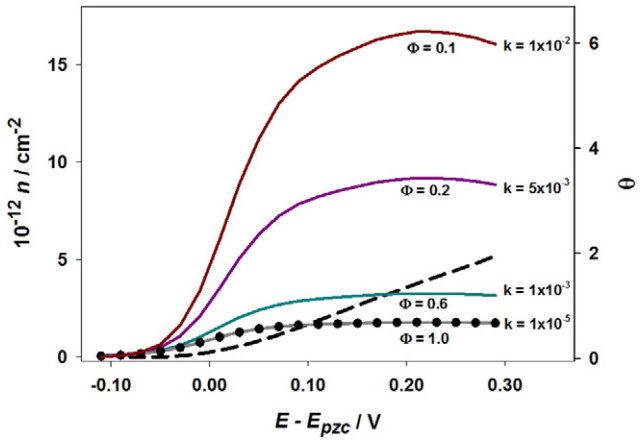

Fig. 5. Particle number density (left) and effective coverage (right) at the liquid/liquid boundary as a function of applied potential estimated from photocurrent responses assuming various values of k_2 (denoted in the graph). Trends estimated from interfacial capacitance (dashed black line) and assuming a perfect quantum yield (Eq. (9), solid circles) are also shown. This analysis is based on data obtained in the presence of Fc, $[TiO_2] = 400\ mg\ L^{-1}$ and $I_0 = 4.7 \times 10^{14}\ cm^{-2}\ s^{-1}$).

the particle surface in sub-picosecond timescale, followed by the generation of hydroxyl radicals and trapped electrons at deep surface states. Considering a characteristic length-scale of the order of the titania lattice constant, second order surface recombination rate constants will translate into values between 0.1 and $5.0 \times 10^{-3}\ cm^2\ s^{-1}$. These results validate our approximations to this complex mechanism, highlighting the interplay between surface recombination at the TiO_2 particles and the heterogeneous rate constant of hole-transfer (mediated by hydroxyl radicals) and electron capture (by dissolved oxygen).

Finally, Fig. 5 also contrasts the potential dependence of n and θ as estimated from the capacitance analysis (Fig. 2). Although absolute values appear close to those obtained from photocurrent data assuming a range of recombination rate constants, the behaviour with respect to potential difference is significantly different. This observation suggests that the underlying assumption used for decoupling the excess charge associated with the TiO_2 particle and the background electrolyte may not be self-consistent. A reason for this discrepancy can be linked to changes in the effective pH at the liquid/liquid boundary due to proton concentration polarization [31,32]. It could be envisaged that the effective charge at the TiO_2 particle increases as the interfacial potential is increased [20]. Another interfacial effect not considered in our analysis involves molecular scale interfacial corrugations associated with capillary waves, which are dependent of interfacial tension and ionic strength [33–35]. To assess these issues, surface sensitive spectroscopic techniques should be considered [36].

4. Conclusions

Photocurrent responses associated with heterogeneous hole-transfer from TiO_2 nanoparticles to a range of hole-acceptors in the organic phase were investigated at the water/DCE interface. Unlike previous studies employing dye species under similar conditions, the magnitude of the photoelectrochemical responses appear unaffected by the formal redox potential of the hole-acceptor in the organic phase. The photocurrent responses (after correction for absorption in the organic electrolyte phase) also showed a non-linear dependence on the photon-flux. This behaviour was rationalized in terms of a mechanism involving heterogeneous-hole transfer (mediated by hydroxyl radicals), electron capture by species in solution (dissolved oxygen), carrier recombination at the nanoparticle surface and a potential dependent coverage of the nanostructures at the ITIES. Considering heterogeneous charge transfer and electron capture in the micro-second time scale, physically plausible coverages were obtained for surface recombination constants of the order of $10^{-3}\ cm^2\ s^{-1}$. These values are consistent with recombination rates estimated by time resolved spectroscopy data.

Acknowledgements

The authors would like to thank Mr. C Manser for preliminary experiments and Mr. KA Bradley for his help with the development of the four-electrode photoelectrochemical set-up, as well as Dr. GR Whittell for insights into ferrocenes, Mr. D Tarling for his talented glassblowing, Mr. DA Davis for elemental analysis and Dr. D Ibañez (Burgos), Mr. FD Eisner and Ms. JJH Humphrey for helpful discussions. The authors gratefully acknowledge the EPSRC (EP/K007025/1) and the School of Chemistry for funding.

Appendix A. Supplementary data

Details regarding the synthesis and characterization of the TiO_2 nanoparticles, as well as UV–vis spectra and three-electrode voltammetry of the various ferrocene-containing organic phases can be found in the supporting information. Supplementary data to this article can be found online at doi:http://dx.doi.org/10.1016/j.jelechem.2015.09.030.

References

[1] Z. Samec, Electrochemistry at the interface between two immiscible electrolyte solutions, Pure Appl. Chem. 76 (2004) 2147–2180.
[2] Z. Samec, et al., Photochemical ion transfer across the interface between two immiscible electrolyte solutions, J. Electroanal. Chem. Interfacial Electrochem. 259 (1989) 309–313.
[3] O. Dvorak, A.H. Dearmond, M.K. Dearmond, Photoprocesses at the liquid liquid interface. 3. Charge-transfer details for photoactive metal-complexes, Langmuir 8 (1992) 508–513.
[4] O. Dvorak, A.H. Dearmond, M.K. Dearmond, Photoprocesses at the liquid liquid interface. 4. Photoxidative transfer with Ru(BPZ)3 2+ complexes, Langmuir 8 (1992) 955–958.
[5] D.J. Fermin, et al., Photocurrent responses associated with heterogeneous electron transfer at liquid/liquid interfaces, Chem. Commun. 1125–1126 (1998).
[6] J.D. Wadhawan, et al., Photoelectrochemically driven processes at the N,N,N′,N′-tetrahexylphenylenediamine microdroplet/electrode/aqueous electrolyte triple interface, J. Solid State Electrochem. 5 (2001) 301–305.
[7] A.M. Collins, et al., Liquid vertical bar liquid vertical bar electrode triple-phase boundary photovoltammetry of pentoxyresorufin in 4-(3-phenylpropyl)pyridine, Langmuir 27 (2011) 6471–6477.
[8] S. Tan, et al., 3D-ITIES supported on porous reticulated vitreous carbon, J. Electroanal. Chem. 604 (2007) 65–71.
[9] M.A. Méndez, et al., Photo-ionic cells: two solutions to store solar energy and generate electricity on demand, J. Phys. Chem. C 118 (2014) 16872–16883.
[10] P. Ge, et al., Photoinduced biphasic hydrogen evolution: decamethylosmocene as a light-driven electron donor, ChemPhysChem 14 (2013) 2308–2316.
[11] X.J. Bian, et al., Floating conductive catalytic nano-rafts at soft interfaces for hydrogen evolution, Chem. Sci. 4 (2013) 3432–3441.
[12] D.J. Fermin, et al., Photoinduced electron transfer at liquid/liquid interfaces. Part III. Photoelectrochemical responses involving porphyrin ion pairs, J. Am. Chem. Soc. 121 (1999) 10203–10210.
[13] N. Eugster, D.J. Fermin, H.H. Girault, Photoinduced electron transfer at liquid vertical bar liquid interfaces: dynamics of the heterogeneous photoreduction of quinones by self-assembled porphyrin ion pairs, J. Am. Chem. Soc. 125 (2003) 4862–4869.
[14] Z. Samec, et al., A generalised model for dynamic photocurrent responses at dye-sensitised liquid/liquid interfaces, J. Electroanal. Chem. 577 (2005) 323–337.
[15] N. Eugster, D.J. Fermin, H.H. Girault, Photoinduced electron transfer at liquid/liquid interfaces. Part VI. On the thermodynamic driving force dependence of the phenomenological electron-transfer hate constant, J. Phys. Chem. B 106 (2002) 3428–3433.
[16] D.J. Fermin, H. Jensen, H.H. Girault, Charge transfer kinetics at liquid/liquid interfaces, in: E.J. Calvo (Ed.), Encyclopedia of Electrochemistry, Wiley-VCH, Weinheim 2003, pp. 360–390.
[17] R.A. Marcus, Theory of electron-transfer rates across liquid liquid interfaces, J. Phys. Chem. 94 (1990) 4152–4155.
[18] I. Benjamin, Y.I. Kharkats, Reorganization free energy for electron transfer reactions at liquid/liquid interfaces, Electrochim. Acta 44 (1998) 133–138.
[19] H.H. Girault, Solvent reorganization energy for heterogeneous electron-transfer reactions at liquid–liquid interfaces, J. Electroanal. Chem. 388 (1995) 93–100.
[20] H. Jensen, et al., Organization and reactivity of nanoparticles at molecular interfaces. Part 1. Photoelectrochemical responses involving TiO(2) nanoparticles assembled at polarizable water vertical bar 1,2-dichloroethane junctions, J. Phys. Chem. B 106 (2002) 10908–10914.
[21] D.J. Fermin, et al., Organisation and reactivity of nanoparticles at molecular interfaces. Part II. Dye sensitisation of TiO2 nanoparticles assembled at the water vertical bar 1,2-dichloroethane interface, ChemPhysChem 4 (2003) 85 (+).

[22] B. Su, et al., Reversible voltage-induced assembly of Au nanoparticles at liquid vertical bar liquid interfaces, J. Am. Chem. Soc. 126 (2004) 915–919.
[23] J. Moser, M. Gratzel, Light-induced electron-transfer in colloidal semiconductor dispersions — single vs dielectronic reduction of acceptors by conduction-band electrons, J. Am. Chem. Soc. 105 (1983) 6547–6555.
[24] A.G. Volkov, Potentials of thermodynamic and free zero charge at the interface between two immiscible electrolytes, Langmuir 12 (1996) 3315–3319.
[25] B. Su, et al., Adsorption and photoreactivity of CdSe nanoparticles at liquid|liquid interfaces, J. Electroanal. Chem. 583 (2005) 241–247.
[26] D.J. Fermin, et al., Photoinduced electron transfer at liquid/liquid interfaces. I. Photocurrent measurements associated with heterogeneous quenching of zinc porphyrins, J. Phys. Chem. B 102 (1998) 10334–10341.
[27] D.W. Bahnemann, M. Hilgendorff, R. Memming, Charge carrier dynamics at TiO2 particles: reactivity of free and trapped holes, J. Phys. Chem. B 101 (1997) 4265–4275.
[28] N. Serpone, et al., Subsecond relaxation dynamics in TiO2 colloidal sols (particle sizes r(p) = 1.0–13.4 nm) — relevance to heterogeneous photocatalysis, J. Phys. Chem. 99 (1995) 16655–16661.
[29] D.E. Skinner, et al., Femtosecond investigation of electron trapping in semiconductor nanoclusters, J. Phys. Chem. 99 (1995) 7853–7856.
[30] D.P. Colombo, et al., Femtosecond study of the intensity dependence of electron-hole dynamics in TiO2 nanoclusters, Chem. Phys. Lett. 232 (1995) 207–214.
[31] R.R. Naujok, et al., Optical 2nd-harmonic generation measurements of molecular adsorption and orientation at the liquid–liquid electrochemical interface, J. Chem. Soc. Faraday Trans. 91 (1995) 1411–1420.
[32] X.L. Zhao, et al., New method for determination of surface pK(a) using 2nd-harmonic generation, Chem. Phys. Lett. 214 (1993) 203–207.
[33] L.I. Daikhin, A.A. Kornyshev, M. Urbakh, Capillary waves at soft electrified interfaces, J. Electroanal. Chem. 483 (2000) 68–80.
[34] L.I. Daikhin, A.A. Kornyshev, M. Urbakh, Effect of capillary waves on the double layer capacitance of the interface between two immiscible electrolytes, Electrochim. Acta 45 (1999) 685–690.
[35] A.A. Kornyshev, M. Urbakh, Direct energy transfer at electrified liquid–liquid interfaces: a way to study interface morphology on mesoscopic scales, Electrochem. Commun. 6 (2004) 703–707.
[36] D.J. Fermin, Linear and non-linear spectroscopy at the electrified liquid/liquid interface, in: R.C. Alkire, et al., (Eds.), Advances in Electrochemical Science and Engineering, Wiley-VCH, Weinheim 2006, pp. 127–161.